water

MDPI

Article

Assessment of the Impacts of Land Use Change on Non-Point Source Loading under Future Climate Scenarios Using the SWAT Model

Mao Feng [1] and Zhenyao Shen [1,2,3,*]

[1] State Key Laboratory of Water Environment, School of Environment, Beijing Normal University, Beijing 100875, China; fdreamg@163.com
[2] Beijing Key Laboratory for Water and Sediment Sciences of Ministry of Education, Beijing 100875, China
[3] Beijing Engineering Research Center for Watershed Environmental Restoration and Integrated Ecological Regulation, Beijing 100875, China
* Correspondence: zyshen@bnu.edu.cn; Tel.: +86-010-588-04733

Abstract: The Miyun Reservoir is an important source of surface drinking water in Beijing. Due to climate change and human activities, the inflow of Miyun Reservoir watershed (MRW) has been continuously reduced in the past 30 years, which has seriously affected the safety of Beijing's water supply. Therefore, this study aimed to assess the mitigation measures based on the quantification of the integrated impacts of climate and land use change in MRW. The non-point source (NPS) model (soil and water assessment tool, SWAT) was used for the development of future climate scenarios which were derived from two regional climate models (RCMs) under two representative concentration pathways (RCPs). Three land use scenarios were generated by the land use model (conversion of land-use and its effects (CLUE-S)): (1) historical trend scenario, (2) ecological protection without consideration of spatial configuration scenario and (3) ecological protection scenario. Moreover, the reduction of sediment and nutrients under three future land use patterns in future climate scenarios was evaluated. The results showed that an appropriate land use change project led to the desired reduction effect on sediment and nutrients output under future climate scenarios. The average reduction rates of sediment, total nitrogen and total phosphorus were 11.4%, 6.3% and 7.4%, respectively. The ecological protection scenario considering spatial configuration showed the best reduction effect on sediment, total nitrogen and total phosphorus. Therefore, the addition of region-specific preference variables as part of land use change provides better pollutant control effects. Overall, this research provides technical support to protect the safety of Beijing's drinking water and future management of non-point source pollution in MRW.

Keywords: climate change; land use change; streamflow; water quality; SWAT; CLUE-S

Citation: Feng, M.; Shen, Z. Assessment of the Impacts of Land Use Change on Non-Point Source Loading under Future Climate Scenarios Using the SWAT Model. *Water* **2021**, *13*, 874. https://doi.org/10.3390/w13060874

Academic Editor: Domenico Cicchella

Received: 18 February 2021
Accepted: 16 March 2021
Published: 23 March 2021

1. Introduction

The non-point source (NPS) pollution has become the main source of pollution in most of China's rivers and lakes, causing the deterioration of water quality [1]. In fact, total nitrogen and phosphorus produced by agricultural NPS pollution have become a constraint to China's sustainable development [2]. It is well known that land use and climate change are two essential factors affecting water quality through NPS progress. In fact, climate change affects the hydrological cycle of the watershed by changing the physical and chemical processes, migration and transformation capacity of pollutants as well as the ability of water bodies to dilute pollutants [3,4], resulting in deteriorating surface water quality and bringing new challenges for the environmental management of watershed [5]. Moreover, land use as a key factor affecting the properties of the underlying surface which determines the basic parameters of the watershed runoff generation and soil erosion processes [6], has a significant impact on the production and output of pollutants

in the soil [7]. Therefore, it is of great significance to study the impacts of land use and climate change on non-point source pollution processes at the watershed scale.

In recent years, various mathematical methods and hydrological climate models have been used to quantify the impact of land use and climate change on watersheds. In future climate scenarios, precipitation and temperature will change, affecting non-point source processes. Zhang et al. [8] estimated the impacts of climate change on streamflow and non-point source pollutant loads by combining the circulation model (HadCM3) with the soil and water assessment tool (SWAT) hydrological model. Narsimlu et al. [9] evaluated the future impacts of climate change on water resources using the SWAT model combined with the sequential uncertainty fitting (SUFI-2) algorithm. Li et al. [10] simulated the changes in NPS pollutant loads for a period of 81 years (2019–2099) by applying the SWAT with six climate model. Numerous studies have also focused on assessing the impact of the land use pattern on NPS pollution. Wang et al. [11] combined the genetic algorithm (GA) with the land use model to achieve an optimized land use pattern to control NPS pollution. The impacts of static and dynamic land use input conditions on the performance of the NPS model and the search for appropriate dynamic land use input to improve model accuracy were also evaluated [12]. The combined impact of climate change and land use were also studied. Moreover, Bai et al. [13] investigated the combined effects of land use and climate change on ecosystem services by using models and environmental setting scenarios where two indicators were developed to evaluate the effects of land use and climate change on these ecosystem services. In addition, Bai et al. [14] used cellular automata (CA) and hydrological models to study the response mechanism of NPS pollution loads to land use change under different precipitation scenarios.

Previous research has indicated that the impacts of global climate change and land use on NPS load are significant; thus, effective management to alleviate the negative effects is indispensable. Furthermore, studies have shown that appropriate mitigation measures can greatly reduce the output of non-point source pollutants [15,16]. For example, Jiang et al. [17] evaluated the reduction of high-level nonpoint source (NPS) pollution discharges in the highland agricultural catchment by applying technical measures using SWAT. In addition, Kaini et al. [18] coupled the genetic algorithm (GA) with SWAT to find an optimal combination of structural measures to meet treatment goals at a watershed scale. Furthermore, Jeon et al. [19] proposed an evaluation methodology to quantify future changes in BMPs on total phosphorus (TP) loads in the river system as a function of climate change.

Over the last 50 years, the measured discharges of the Haihe River Watershed have shown a significant decrease resulting from the impact of human activities and climate change. In fact, the inflow of the Miyun Reservoir, which is the largest reservoir in the Haihe River Watershed, has been continuously reduced in the past 30 years. Indeed, climate change contributed 25% and 45% to the reduction of runoff from the main rivers entering the Miyun Reservoir—the Chaohe River and Baihe River respectively, which seriously affected the water supply safety and sustainable development of Beijing [20]. At present, the eutrophication degree of Miyun Reservoir is mesotrophic and the tendency to eutrophication is evident [21] and agricultural non-point source pollution has become the main factor affecting the water quality of Miyun Reservoir. Therefore, it is of great significance to study the impact of climate change and human activities on the hydrology and ecology of the watershed [22].

On the other hand, previous studies mentioned above have certain limitations, such as the use of future climate data from old emission scenarios data source. Moreover, future land use scenarios did not consider spatial allocation, resulting in uncertainties in the assessment of impacts on hydrology and water quality. Therefore, in this paper we evaluated the non-point source control strategy and the pollutant reduction effect in the context of land use change under future climate scenarios with SWAT model. The main objectives of this study were: (1) to estimate the future climate change by quantile mapping methods (2) to analyze the land use change pattern of the past, present and future by CLUE-S model;

(3) to estimate the stream flow and nutrient loading under climate change; (4) to investigate the impact of the characteristics of land use change patterns on streamflow and nutrient loading in future climate scenarios. This research presents a certain theoretical and practical significance for the future non-point source pollution control and management and urban drinking water safety. It also provides a management model for future non-point source pollution under climate change conditions in other river watersheds.

2. Materials and Methods

2.1. Study Area

MRW refers to the Chaohe and Baihe rivers controlled by the Miyun Reservoir. The watershed area is 15,400 km^2 and belongs to the Haihe River system, which is located at 40°19′–41°38′ north latitude and 115°25′–15°35′ east longitude and is shown in Figure 1. The vegetation cover in the watershed with forest and grassland reaching 76% and arable land accounting for about 21%. The main types of vegetation are woodlands, grasslands and cultivated land. Among them, broad-leaved forests accounted for the most, representing 39.37% of the total area; bare fields followed, representing 17.65% and natural grasslands representing 14.23% of the total area.

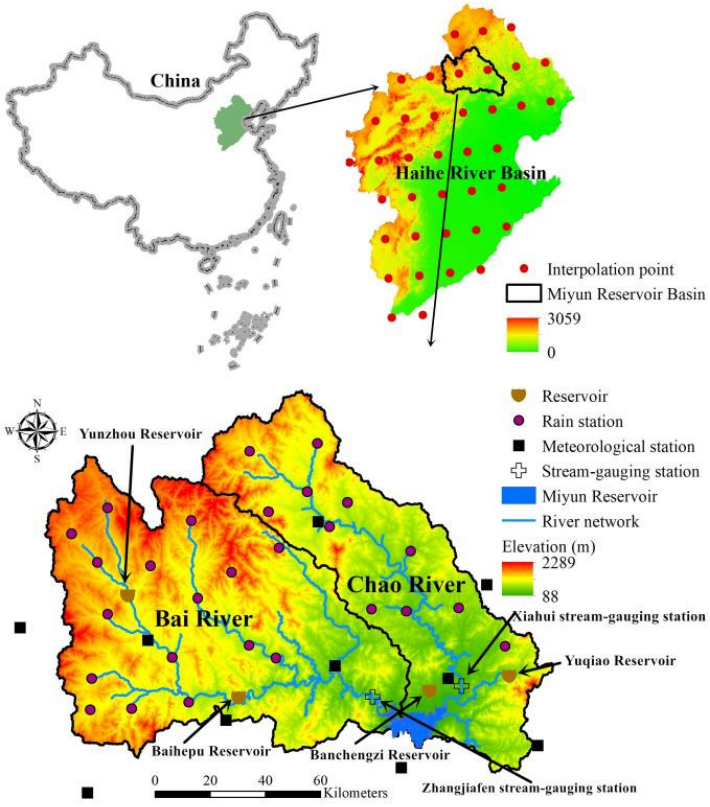

Figure 1. Location of the Miyun Reservoir Watershed (MRW) and hydroclimatic stations.

2.2. Data Collection

Historical Meteorological data used in this study include precipitation, temperature and relative humidity; hydrological data include runoff, sediment and water quality; spatial geographic data includes DEM, soil and land use (Table 1). Future climate change data are mainly monthly scale precipitation and temperature output data from IPCC GCMs, 44 GCMs containing future climate change scenario data are selected which comes from the IPCC Data Distribution Center website (http://www.ipcc-data.org/, accessed on 18 March 2021), and the time periods are 1961–2004, 2020–2042 and 2060–2082. Runoff and sediment data were collected from the two hydrological stations closest to the entrance of the Miyun Reservoir and the hydrological station of Xiahui and Zhangjiafen, includ-

ing monthly runoff data from 1969 to 2012, monthly sediment data from 1988 to 2008 and daily runoff data from 1969 to 1979. The digital elevation data was provided by the international scientific data service platform with a resolution of 30 × 30 m^2. The land use data were obtained from the Resource and Environmental Science Data Center of the Chinese Academy of Sciences, including land use in 1980, 2000 and 2008, which are mainly divided into six categories: farmland, forest, grassland, water area, unused land, urban and rural land, industrial and mining residential land. The soil data were identified from the 1:10,000,000 scale soil map of the People's Republic of China and edited by the Nanjing Soil Research Institute.

Table 1. Land use structure and single land use dynamics values during 2000–2008.

Land Use Type	2000		2008		2000–2008 Annual Rate of Change (%)
	Area (hm^2)	Proportion (%)	Area (hm^2)	Proportion (%)	
Forest	755,689	49.21	757,623	49.33	0.03
Grassland	414,709	27.00	413,809	26.94	−0.03
Water body	28,757	1.87	28,658	1.87	−0.04
Urban land	8780	0.57	9268	0.60	0.69
Unused land	2334	0.15	2287	0.15	−0.25
Farmland	325,491	21.19	324,115	21.10	−0.05

The datasets were used to generate future climate change scenarios in the watershed and to initialize the SWAT model and the CLUE-S model.

2.3. Historical Land Use Change

Analysis of the changes in the land use structure in the study area can provide a basis for establishing land use conversion rules and building future land use scenarios. Changes in land use structure in MRW mainly include the total amount of changes, the variation rate, the conversion relationship and the amount of conversion between different land use types. Table 1 shows that the land use structure did not change significantly in the study period (from 2000 to 2008). The three main land use types remain farmlands, forests and grasslands, which account for 97% of the watershed area and there was little difference in the spatial distribution between the different land use types. Among them, the farmland is mainly distributed in the western part of the study area (Chicheng County), the northeastern and the northern part of Miyun Reservoir. From the perspective of single land use dynamics, from 2000 to 2008, forests and urban lands showed an increasing trend and urban lands changed drastically; while grasslands, water bodies, unused lands and arable lands showed a downward trend, in which unused land changed drastically. The land use matrix (Table 2) was constructed based on the land use changes revealing the transformation and dynamic changes between different land use types.

Table 2. Transition matrix of different land use types during 2000–2008.

Land Use	Farmland	Forest	Grassland	Water Body	Building Land	Unused Land
Farmland	258,199.6	24,567.0	36,784.1	4004.6	2475.4	77.9
Forest	19,689.0	696,492.3	43,751.8	1235.1	537.2	151.0
Grassland	42,513.1	40,151.6	325,528.0	931.8	359.0	402.6
Water body	3452.4	1204.5	1523.4	21,342.1	96.8	1.8
Building land	2111.0	268.8	205.3	120.0	4911.7	0.0
Unused land	125.6	158.5	299.9	21.0	0.0	1617.6

2.4. Research Methodology

2.4.1. Future Climate Data Corrected by Quantile Mapping Methods

Due to the large deviation of the spatial resolution of GCMs and the simulation of meteorological elements, the output results need to be post-processed before they can be used. Statistical downscaling methods are widely used in climate change impact

research due to their high computational efficiency [23–27]. This research uses a bilinear interpolation method to interpolate GCMs grid point data to precipitation and temperature observation stations in the watershed and then uses the quantile mapping method to establish a conversion function between model output and observations and apply the conversion function to future models for predicting results. Studies have shown that the QM method has a good bias correction effect and can well retain the original statistical characteristics of the data [28,29]. This method has a wide range of applications in the field of climate change impact research. The specific formula is presented as follows:

$$\widetilde{x}_{m-p,adjst} = F_{o-c}^{-1}\left(F_{m-c}\left(x_{m-p}\right)\right) \quad (1)$$

Among them, F is the cumulative distribution function of the observed value (o) or simulated value (m) of the current climate (c) or future forecast period (p) and the subscript o-c represents the current climate observation.

In this paper, the QM method was used with two typical emission scenarios (RCP4.5, RCP8.5) and two GCMs to generate future climate scenario data for the Miyun Reservoir watershed according to literature [30].

2.4.2. Land Use Change Model

This paper uses the conversion of land use and its effects (CLUE-S) model to analyze the impact of future land use changes on the output of non-point source pollution in the watershed [31]. The CLUE-S model includes a non-space requirement module and a space intuitive allocation module. Through spatial analysis and dynamic simulation, the spatial allocation module transforms the overall change of the entire land use type area into land use changes in different locations or different spaces based on a grid system. The information inquired to run the spatial allocation module includes spatial policies and regional land use restrictions, conversion parameters between land use types, land use requirements and location characteristics.

The calculation formula can be expressed as follows:

$$\mathrm{Log}\left(\frac{P_i}{1-P_i}\right) = \beta_0 + \beta_1 X_{1,i} + \beta_2 X_{2,i} \cdots\cdots + \beta_N X_{n,i} \quad (2)$$

$$TPROP_{i,u} = P_{i,u} + ELAS_u + ITER_u \quad (3)$$

$TPROP_{i,u}$: The total probability of the u-th land use type in grid unit i according to the formula.

Among them, $P_{i,u}$ is the total probability of the u-th land use type at location i based on the logistic regression model, $ELAS_u$ is the conversion elasticity coefficient of the u-th land use type and $ITER_u$ is an iterative variable for land use types that explains the relative competitive advantage between different land types. The iterative variables $ITER_u$ of all land use types have the same value.

Based on the land use map of the MRW in 2000 with 10 selected driving factors, the CLUE-S model is used to simulate the land use distribution pattern in 2008. The parameter files required for the model include: the initial year land use map, the regional constraint file, the land use demand file, etc. This paper uses Kappa index to quantitatively evaluate the accuracy of CLUE-S simulation results in 2008. The Kappa index value generally ranges from 0 to 1. When 0.4 < Kappa < 0.75, the agreement between the two is general; When Kappa > 0.75, the agreement between the two is better; the closer the value is to 1, the higher the accuracy of the simulation result.

2.4.3. Hydrological and Water Quality Modeling

The soil and water assessment Tool (SWAT) is a physically based and continuously distributed hydrological model. It is widely used to investigate the long-term impacts of land management practices, climate variability and land-use changes on hydrological progress [32]. The water balance is calculated at the hydrological response units (HRUs)

level, aggregated at the sub watershed level and finally, routed to the reaches and the watershed outlet. The water balance is calculated as follows:

$$SW_t = SW_0 + \sum_{i=1}^{t}\left(R_{day} - Q_{surf} - E_a - W_{seep} - Q_{gw}\right) \quad (4)$$

where SW_t is the final soil moisture content of day i, SW_0 is the initial soil moisture content of day i, R_{day} is the rainfall of day i, Q_{surf} is the surface runoff of day i, E_a is the evapotranspiration of day i, W_{seep} is the water transferred from soil profile into the gas zone of day i and Q_{gw} is the return flow of day i.

In this study, the reference period refers to the historical simulation period from 1988 to 2010, the future evaluation period is divided into two stages: 2020–2042 and 2060–2082. The future climate scenario data were entered into the calibrated SWAT model and performed simulations of non-point source pollution in the watershed under different climate change scenarios. By comparing with the reference period, the characteristics of change in the output of non-point source pollution over different future assessment periods were evaluated. In the future simulation process, the land use type will remain the land use type map from 2000, used in the historical simulation period.

3. Results and Discussion

3.1. Model Calibration and Validation

3.1.1. SWAT Model Calibration and Validation

The simulation results of runoff and total nitrogen at the two stations are shown in Figure 2. The water quality evaluation indicators (R^2 and NSE value) during the verification period were lower than the regular water quality evaluation indicators. The results of calibration for the SWAT parameters in the Baihe and Chaohe watersheds are shown in Table 3. The calibrated SWAT model can accurately describe the process of hydrological cycle and the process of migration and transformation of pollutants in the watershed. It can also be used to analyze the impact of climate change and land use change scenarios on the runoff and aquatic environment of the watershed.

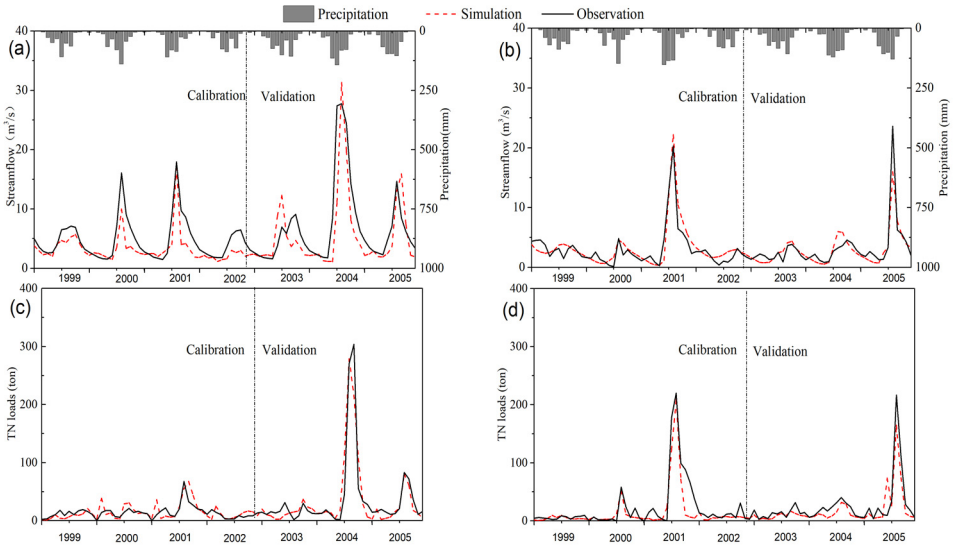

Figure 2. Observed and simulated daily streamflow and total nitrogen (TN) loads from 1999 to 2005. (**a**) The observed and simulated daily streamflow in Baihe River; (**b**) The observed and simulated daily streamflow in Chaohe River; (**c**) The observed and simulated total nitrogen in Baihe River; (**d**) The observed and simulated daily streamflow in Chaohe River.

Table 3. Performance of the Soil and Water Assessment Tool (SWAT) simulation in the watershed.

Variable	Time Period	Chaohe River		Baihe River	
		R^2	Ens	R^2	Ens
Streamflow	Calibration (1999–2002)	0.851	0.848	0.908	0.906
	Validation (2003–2005)	0.856	0.809	0.754	0.745
Total Nitrogen	Calibration (1999–2002)	0.798	0.763	0.865	0.737
	Validation (2003–2005)	0.505	0.389	0.573	0.142

3.1.2. CLUE-S Model Calibration and Validation

The CLUE-S model was initialized after setting all the model parameter files. After many iterations, a land use simulation map in 2008 was obtained. The Kappa index was calculated by analyzing the CLUE simulation results using land use status map from 2008. The Kappa index was 0.67, indicating that the accuracy of the model simulation results can reach 67%. Depending on the level of consistency of the Kappa index, the results of the CLUE-S simulation of the Miyun Reservoir watershed in 2008 and the results of the historical land use status map were highly consistent. Thus, we can assume that the simulation results of the CLUE-S model have high credibility and that the calibrated model can be used for the analysis of future land use change scenarios.

3.2. Future Climate Change Analysis

According to the performance evaluation results and data availability of 44 CMIP5 GCMs in the Haihe River Basin in precipitation and average temperature [33], two climate models (ACCESS1.3 and HadGEM-ES) and two typical emission scenarios (RCP4.5 and RCP8.5) were used to predict future trends in precipitation and temperature in the Miyun Reservoir watershed during two future evaluation periods (2020–2042 and 2060–2082), which were compared with the base period (1988–2010).

3.2.1. Variation in Future Temperature

The average maximum temperature and the 95th value of the Miyun Reservoir watershed are shown in Figure 3. Compared with the average maximum temperature of the MRW (13.5 °C) during the base period, the future maximum temperature under the two emission scenarios of RCP4.5 and RCP8.5 showed an increasing trend. The variations in the maximum temperature under different emission scenarios were obviously different. Indeed, the temperature under RCP8.5 scenario from 2060 to 2082 showed an annual increase of 4.5 °C, which was the highest. This variation was essentially the same as that of the greenhouse gas emission scenario in which, higher greenhouse gas emissions led to a greater temperature increase. From the perspective of the future maximum temperature generated by different GCMs, the maximum temperature variation generated by the HadGEM-ES model was the largest under the same emission scenario and evaluation period. The 95th value of the highest temperature in the base period was 30.3 °C and the 95th value of the highest temperature under different climate combinations showed an increasing trend. Among them, the temperature increase was the largest under RCP8.5 scenario from 2060 to 2082 with a value of 5.2 °C. Like the average maximum temperature, the HadGEM-ES model generated the largest change in maximum temperature under the same emission scenario and evaluation period. In order to better describe changes in future maximum temperature and to reduce prediction uncertainty, the ensemble average method was used to reflect future changes in maximum temperature in the watershed. During 2020–2042, the average maximum temperature will increase by 1 °C and 1.4 °C, whereas during 2060–2082, it will increase by 2.5 °C and 4.1 °C under RCP4.5 and RCP8.5 scenarios, respectively.

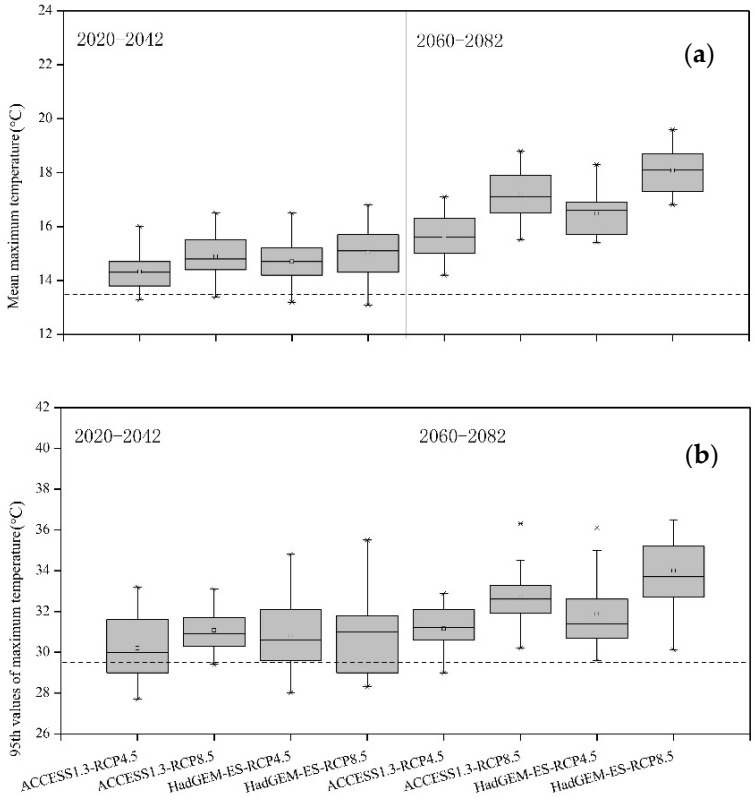

Figure 3. (**a**) Projected mean and (**b**) 95th values of maximum temperature under the different combinations of General Circulation Models (GCMs) and Representative Concentration Pathways (RCPs) scenarios during the different assessment periods.

Figure 4 shows the predicted values of the monthly and seasonal averages of the highest temperature in the MRW under different combination scenarios. As can be seen in the next two evaluation periods, the two climate models ACCESS1.3 and HadGEM-ES will show a warming trend at both monthly and seasonal time scales, which is consistent with the change trend of the annual maximum temperature. In different evaluation periods in the future, the monthly and seasonal average rates of the highest temperature increase in the period from 2060 to 2082 will be significantly higher than those in the period from 2020 to 2042. It is noteworthy that the rise in the maximum temperature in spring and winter was greater than that in summer and autumn.

The average minimum temperature and the 5th value of the MRW are shown in Figure 5. Compared with the annual average minimum temperature (0.8 °C) during the base period, the future minimum temperature in the MRW under RCP4.5 and RCP8.5 showed an increasing trend and the variations in the minimum temperature under different emission scenarios were obviously distinct. Among them, during the period from 2060 to 2082, the temperature increase was greatest under RCP8.5 scenario with a value of 5.3 °C, which was basically consistent with the trend of temperature variation under the greenhouse gas emission scenario. From the perspective of the future minimum temperature generated by different GCMs, the HadGEM-ES model generated the biggest change in the minimum temperature under the same emission scenario and evaluation period. The 5th value of the lowest temperature in the base period was −17.6 °C and the 5th value of the lowest temperature in the MRW under different climate combinations showed an increasing trend. Among them, the temperature increase was the highest under RCP8.5 scenario from 2060 to 2082 with a value of 6.1 °C. Under RCP4.5 scenario from 2020 to 2042, the minimum temperature of the ACCESS1.3 climate model had the largest variation of 5th, while under RCP8.5 scenario, the HadGEM-ES climate model had the greatest change. During the period from 2060 to 2082, the minimum temperature generated by the ACCESS1.3

model under RCP4.5 and RCP8.5 scenarios had the largest change in the 5th. The ensemble average method was also used to reflect the future minimum temperature changes in the watershed. During 2020–2042, the average minimum temperature increase will be 1.4 °C and 1.7 °C, whereas during 2060–2082, it will be 3.2 °C and 5.9 °C, under RCP4.5 and RCP8.5 scenarios, respectively.

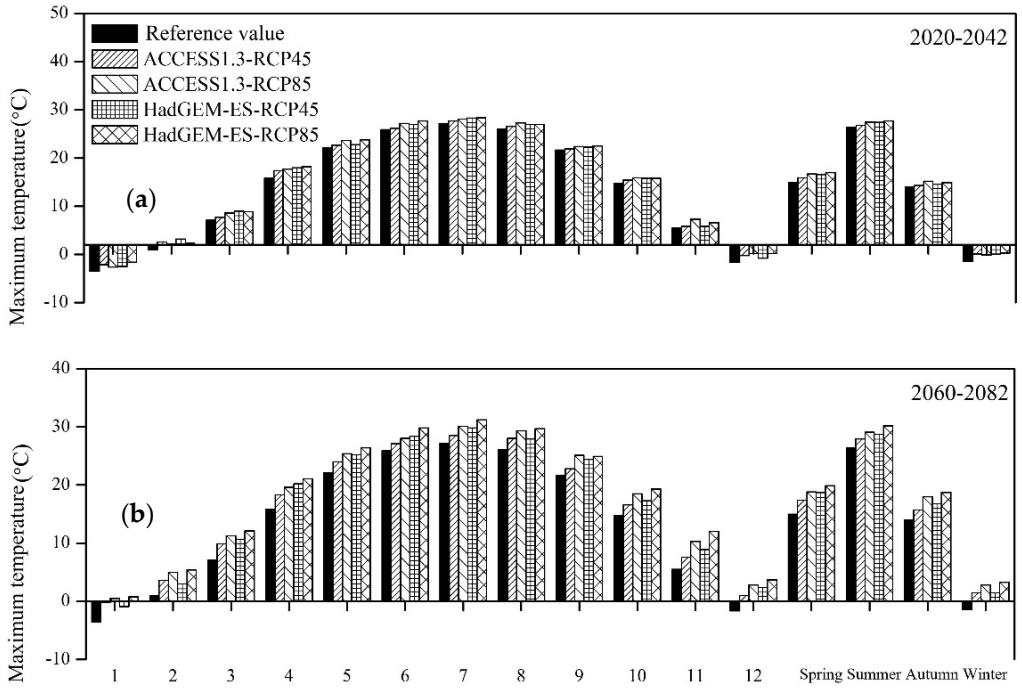

Figure 4. Projected values of maximum temperature under the different combinations of GCMs and RCPs scenarios during the different assessment periods. (**a**) from 2020 to 2042; (**b**) from 2060 to 2082.

Figure 6 shows the predicted values of the monthly and seasonal averages of the minimum temperature in the MRW under different combination scenarios. It was depicted that in the next two evaluation periods, ACCESS1.3 and HadGEM-ES will show a warming trend at monthly and seasonal time scales, which is consistent with the change trend of the annual minimum temperature. In different evaluation periods in the future, the monthly and seasonal average rates of the minimum temperature in the period from 2060 to 2082 will increase significantly more than those in the period from 2060 to 2082. Note that the minimum temperature increase in spring and winter was higher than that in summer and autumn.

3.2.2. Variation in Future Precipitation

The annual precipitation in the MRW is shown in Figure 7. During 2020–2042, the annual average precipitation will increase by 17.1 mm and 16.9 mm, whereas during 2060–2082, it will increase by 33.7 mm and 50.6 mm, under RCP4.5 and RCP8.5 scenarios, respectively.

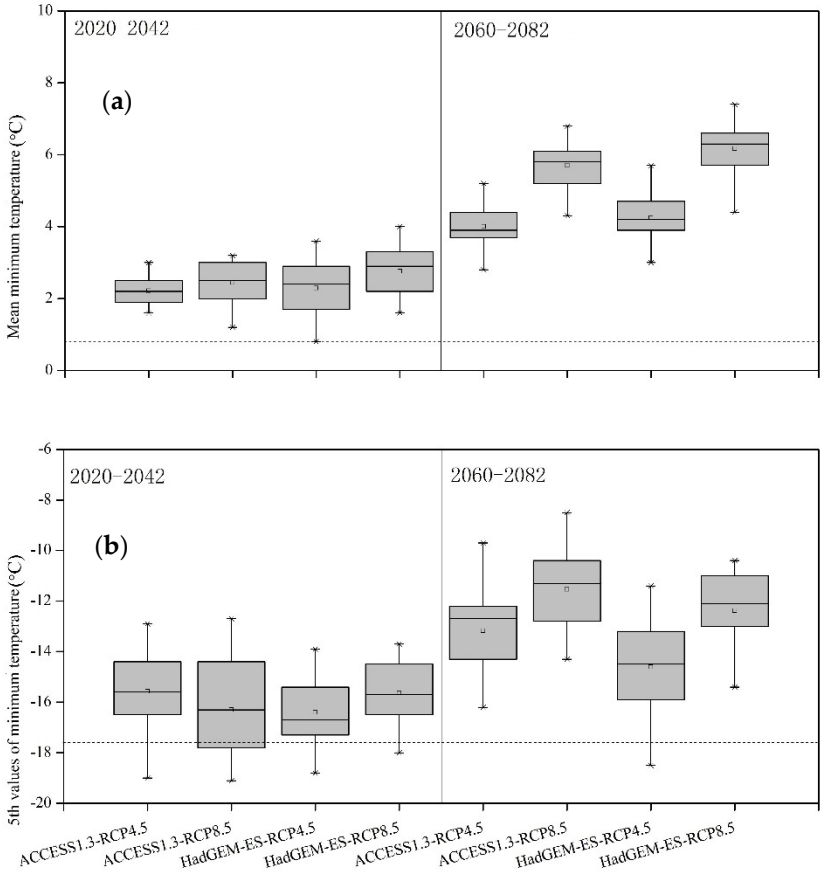

Figure 5. (**a**) Projected mean and (**b**) 5th values of minimum temperature under the different combinations of GCMs and RCPs scenarios during the different assessment periods.

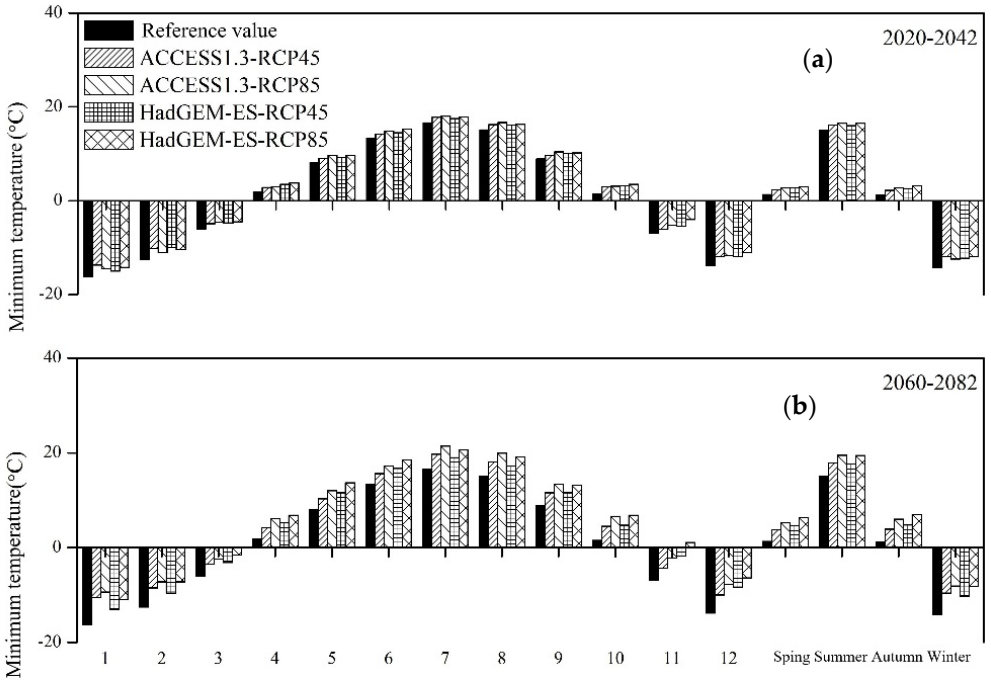

Figure 6. Projected values of minimum temperature under the different combinations of GCMs and RCPs scenarios during the different assessment periods (**a**) from 2020 to 2042; (**b**) from 2060 to 2082.

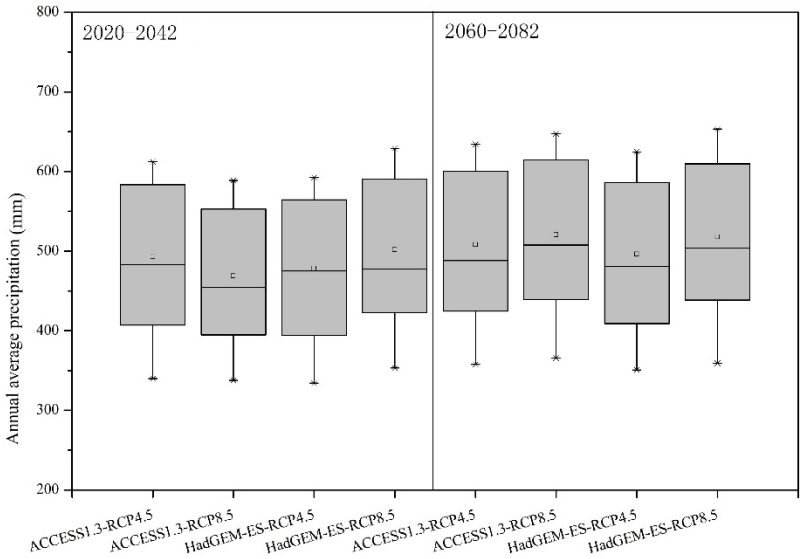

Figure 7. Projected mean of precipitation under the different combinations of GCMs and RCPs scenarios during the different assessment periods.

Figure 8 shows the predicted values of the monthly and seasonal averages of precipitation in the MRW under different combination scenarios. Compared with the maximum and minimum temperatures, the future changes in precipitation will be much more complicated. At monthly time scale, the five monthly precipitations of 1, 2, 8, 9 and 10 all showed an increasing trend under different climate combinations. Autumn and winter precipitation also showed an increasing trend.

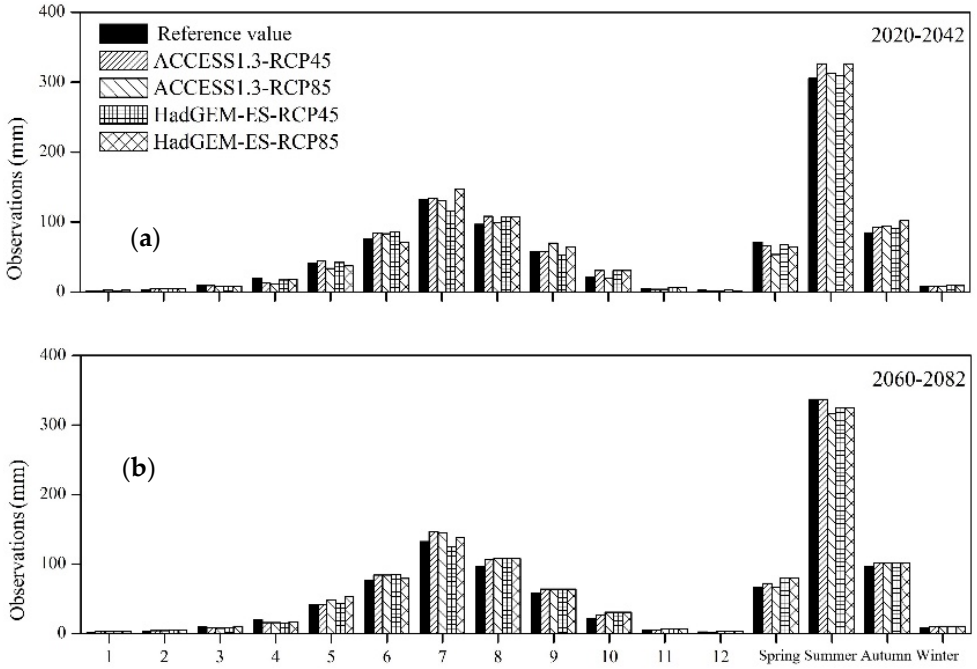

Figure 8. Projected mean of precipitation under the different combinations of GCMs and RCPs scenarios during the different assessment periods (**a**) from 2020 to 2042; (**b**) from 2060 to 2082.

According to the empirical downscaling method, the future climate of the MRW will show a trend of warming and humidification, which is consistent with the results obtained by Bao et al. [34] and the future climate change of the Haihe River Watershed [35]. All GCMs and RCPs showed that the annual and monthly maximum and minimum temperatures in

the Miyun Reservoir watershed will gradually increase. Unlike temperature, future changes in precipitation at the monthly scale will be bidirectional and will depend on the GCMs selected and the evaluation time period. The two-way change in precipitation may be attributed to the simulation ability of GCM, because the precipitation simulation of different GCMs may be inconsistent with the magnitude and direction of the change in a specific area.

3.3. Climate Change Impact on Streamflow and Sediments

The spatial distribution of runoff changes in the watershed under different climate scenarios is shown in Figure 9. At different time periods, watershed runoff varied greatly under greenhouse gas emission scenarios and global climate models. From 2020 to 2042, the reduction of watershed flow mainly occurred in the upper and middle reaches of the Chaohe and Baihe Rivers with a range of variation of 0–10 mm under ACCESS1.3-RCP8.5 and HadGEM-ES-RCP4.5 scenarios. Under the two other models, the runoff of the watershed basically showed an increasing trend. The sub-watershed runoff increased by 20 mm mainly concentrated in the lower reaches of the Chaohe and Baihe Rivers, compared with the base period watershed runoff basically showed an increasing trend at the sub-watershed level (from 2060 to 2082). Sub-watersheds with increasing runoff were mainly found in No. 27, 32 and 34 sub-watersheds of the Baihe River Watershed and No. 19, 20 and 22–29 sub-watersheds of Chaohe River.

The spatial distribution of sediment changes in the watershed under different climate scenarios is shown in Figure 10. The sediment yield of the river watershed varied significantly under the different emission scenarios and global climate models over the different evaluation periods. From 2020 to 2042, the sediment yield in the watershed under ACCESS1.3-RCP4.5 and HadGEM-ES-RCP8.5 scenarios, basically showed an increasing trend concentrated in the 23rd sub-watershed of the Baihe River and in the 15th and 23rd of the Chaohe River. The 29th sub-watershed under ACCESS1.3-RCP8.5 and HadGEM-ES-RCP4.5 scenarios showed greater spatial differences in sediment yield in the watershed. Sediment yield in 13 sub-watersheds within the ACCESS1.3-RCP8.5 watershed was reduced, ranging from -0.484 to -0.001 kg/ha, with an average value of -0.06 kg/ha. Under HadGEM-ES-RCP4.5 scenario, there were 33 sub-watersheds in the watershed with reduced sediment yield output changes, ranging from -0.597 to -0.007 kg/ha, with an average value of -0.1 kg/ha; during the period from 2060 to 2082, the sediment yield in the watershed showed an increasing trend at the sub-watershed level. Compared with the base period, the sub-watersheds with an increase of more than 1 ton/ha of sediment yield in the sub-watershed were mainly distributed in the middle and lower reaches of the Chaohe River and the west of the Baihe River. The sub-watersheds with increased sediment yield in the future were mainly the No. 23 sub-watersheds of the Baihe River Watershed and the 5, 15, 16, 20, 23–25, 28 and 29 sub-watersheds of Chaohe River.

Figure 11 depicts the spatial distribution changes in the total nitrogen loading in the watershed under different climate scenarios. The total nitrogen load of the watershed varied greatly with the different emission scenarios and global climate models. From 2020 to 2042, the changes in total nitrogen load in the sub-watershed within the watershed, under ACCESS1.3-RCP4.5 and HadGEM-ES-RCP8.5 scenarios, showed an overall increasing trend. The watershed total nitrogen load increased mainly in Chaohe 17, Sub-watersheds 19, 20, 23, 24 and 28. Under ACCESS1.3-RCP8.5 and HadGEM-ES-RCP4.5 scenarios, the spatial difference in the total nitrogen load in the watershed was relatively large. Among them, under HadGEM-ES- RCP4.5 scenario, the total nitrogen load of 29 sub-watersheds in the watershed decreased, ranging from -0.707 to -0.008 kg/ha, with an average value of -0.12 kg/ha; during the period from 2060 to 2082, the total nitrogen load in the watershed showed an increasing trend at the sub-watershed level. Compared with the base period, the sub-watersheds with a variation in total nitrogen load of more than 1 kg/ha in the sub-watershed were distributed mainly in the upper and lower reaches of the Chaohe River and in the middle part of the Baihe River. Specifically, these sub-watersheds were the

18 sub-watersheds of the Baihe River Watershed and the 1, 5–8, 15–17, 19, 20, 23–25 and 28 sub-watersheds of Chaohe River.

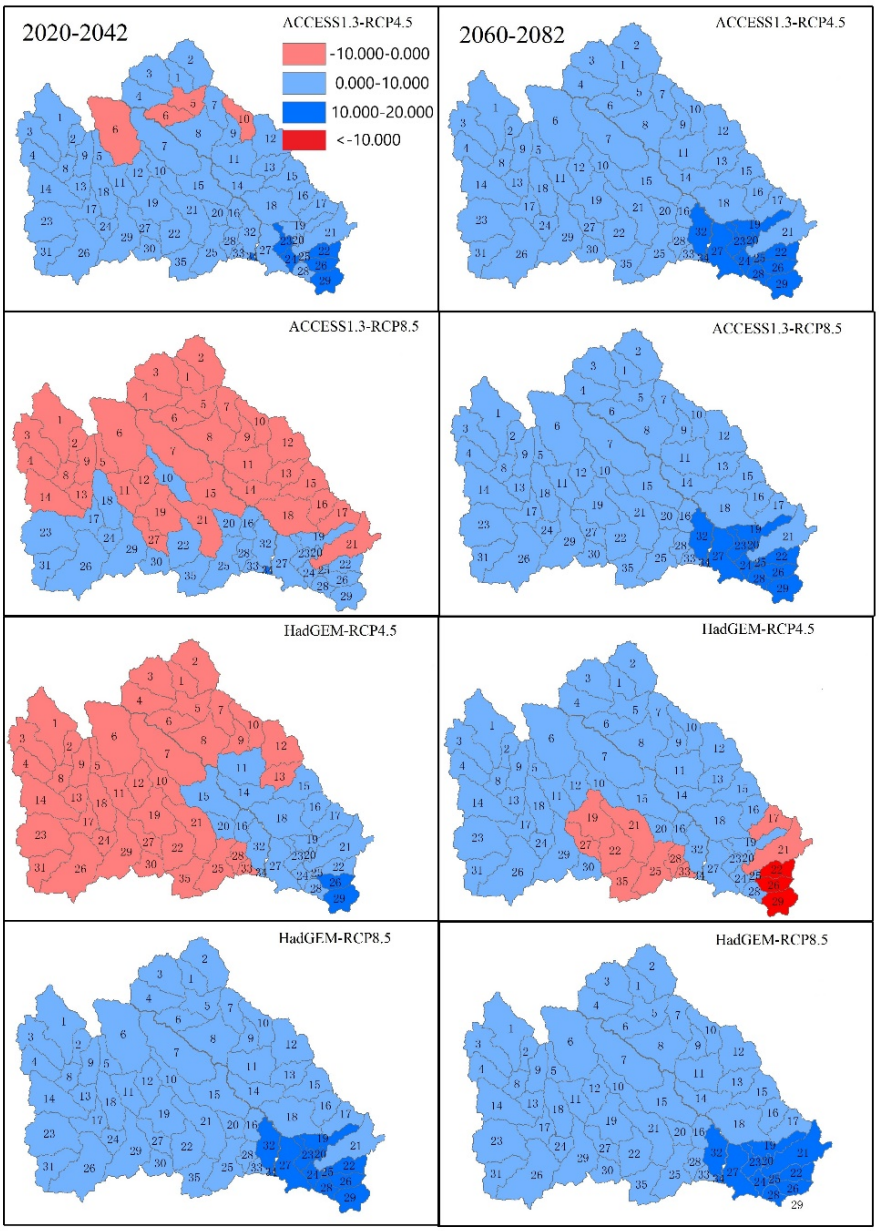

Figure 9. Spatial distribution of water yield under different climate change projections.

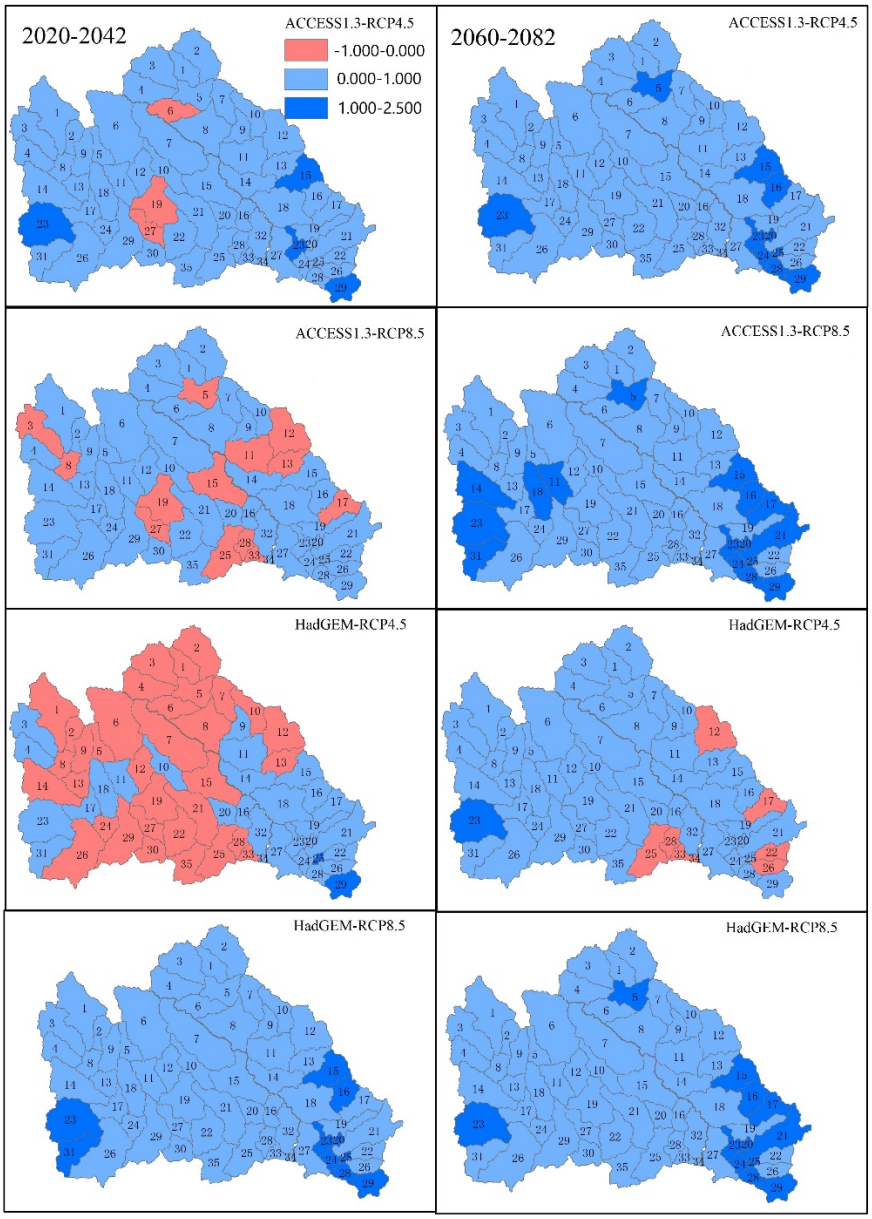

Figure 10. Spatial distribution of sediment load under different climate change projections.

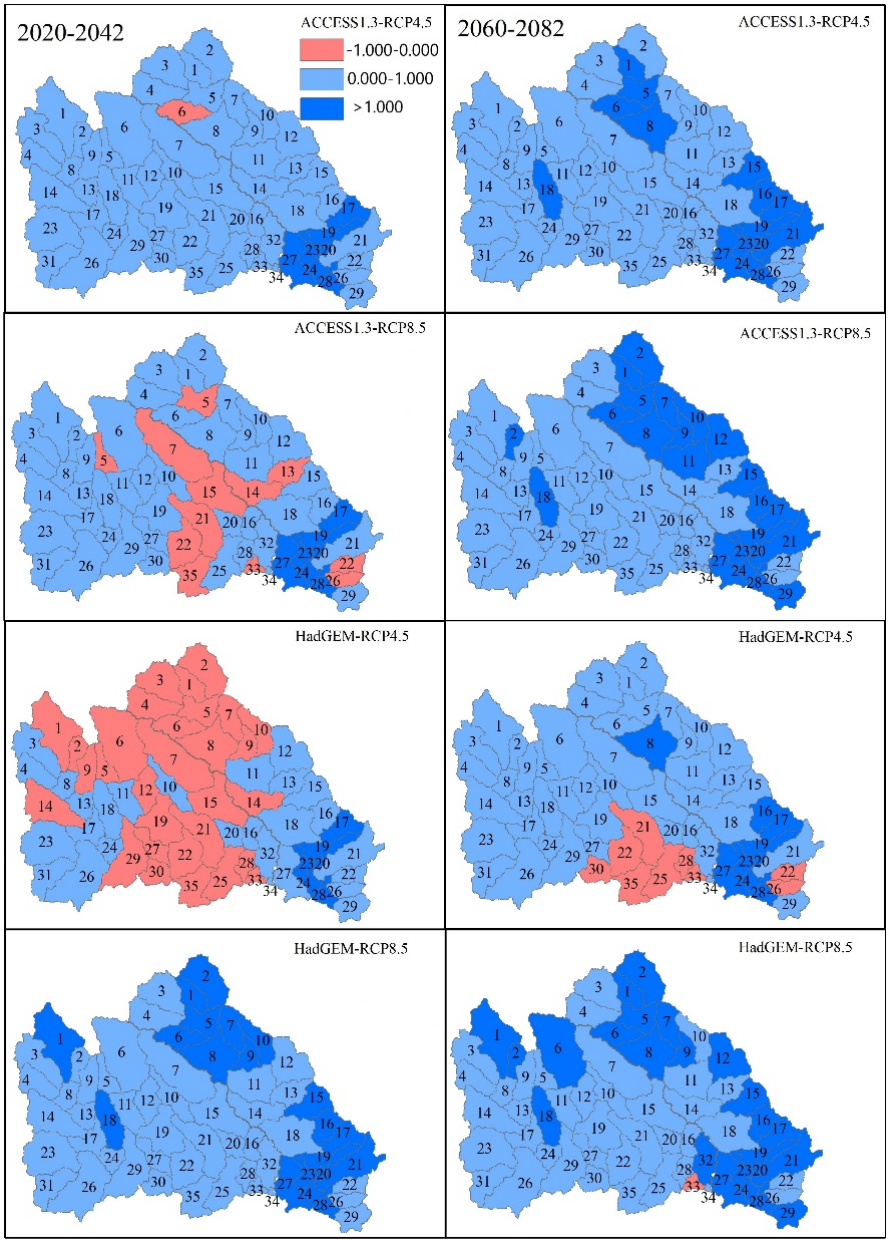

Figure 11. Spatial distribution of total nitrogen under different climate change projections.

Figure 12 depicts the spatial distribution of changes in total phosphorus load in the watershed under different climate scenarios. The total phosphorus load in the watershed varied considerably under different emission scenarios and global climate models. From 2020 to 2042, the variation in total phosphorus load in watershed sub-catchments under ACCESS1.3-RCP4.5, ACCESS1.3-RCP8.5 and HadGEM-ES-RCP8.5 scenarios showed an increasing trend and sub-catchments with a total variation in phosphorus output greater than 0.021 kg/ha were the No. 23 sub-watersheds of Baihe River and No. 15–17, 23 and 29 sub-watersheds of Chaohe River. For HadGEM-ES-RCP4.5 scenario, there were 22 sub-watersheds in the watershed showing a decreasing trend, ranging from −0.014 to −0.001 kg/ha, with an average value of −0.004 kg/ha; during the period from 2060 to 2082, the total phosphorus load in the watershed was maintained on an increasing trend at the sub-watershed level. Compared with the base period, the sub-watersheds with a total variation in phosphorus load greater than 0.021 kg/ha were distributed mainly in the middle and lower reaches of the Chaohe River and in the western part of the Baihe River.

Specifically, these sub-watersheds were No. 6, 10, 14 and 23 of the Baihe River Watershed and No. 2, 5, 6, 12, 15–17, 19–21, 23–25, 28 and 29 of Chaohe River. Sub-watershed.

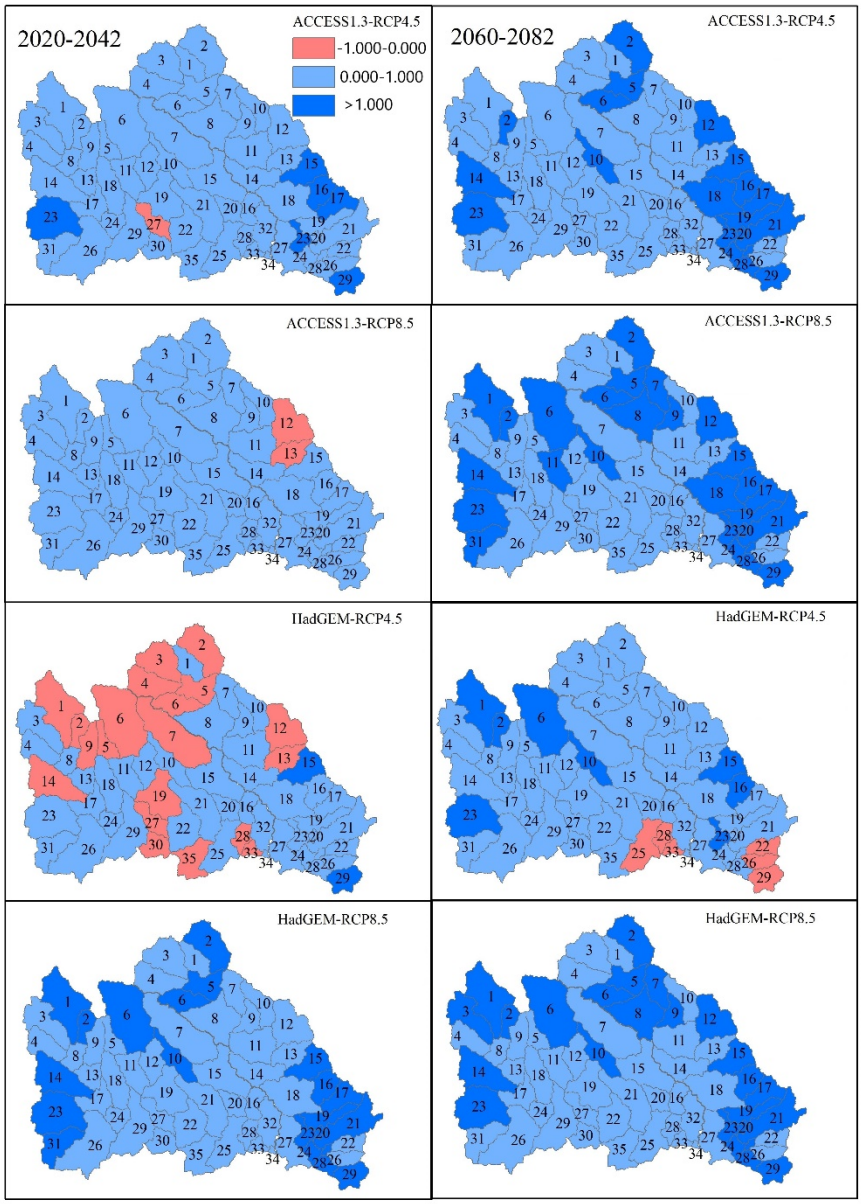

Figure 12. Spatial distribution of total phosphorus under different climate change projections.

Table 4 describes watershed evaporation, runoff, total nitrogen and total phosphorus loading over different future evaluation periods by collective average. The results in the future evaluation, were all greater than the values of the corresponding variables in the reference period and the range of changes in the variables from 2060 to 2082 was greater than that in the 2020 to 2042 period.

Table 4. Evapotranspiration, water yield, total nitrogen and total phosphorus loads of the land phase in the future.

Variable	Base Period (1988–2010)	Evaluation Period 1 (2020–2042)		Evaluation Period 2 (2060–2082)	
		RCP4.5	RCP8.5	RCP4.5	RCP8.5
Evaporation (mm)	429.1	438.7 437.6	436.2 435.0	452.5 450.5	466.5 461.3
Runoff (mm)	46.61	48.47 49.32	50.45 51.37	51.13 52.84	54.46 58.56
Sediment (10^4 ton/ha)	1.05	1.198 1.220	1.382 1.379	1.470 1.474	1.619 1.708
Total nitrogen (ton/ha)	1.20	1.401	1.691	1.723	1.905
Total phosphorus (ton/ha)	0.03	0.0360 0.0363	0.0419 0.0418	0.0448 0.0443	0.0494 0.0506

Figure 13 depicts the estimated monthly average discharge, sediment, total nitrogen and total phosphorus loadings under different future climate change scenarios. It can be seen that there was no significant change in these parameters from January to May and December. Concerning the future change in the precipitation in the river watershed, it will be mainly concentrated in the flood season. Under HadGEM-ES-RCP8.5 climate scenario, runoff, sediment and total phosphorus decreased in July during 2020–2042 and 2060–2082 but showed an increasing trend in other months.

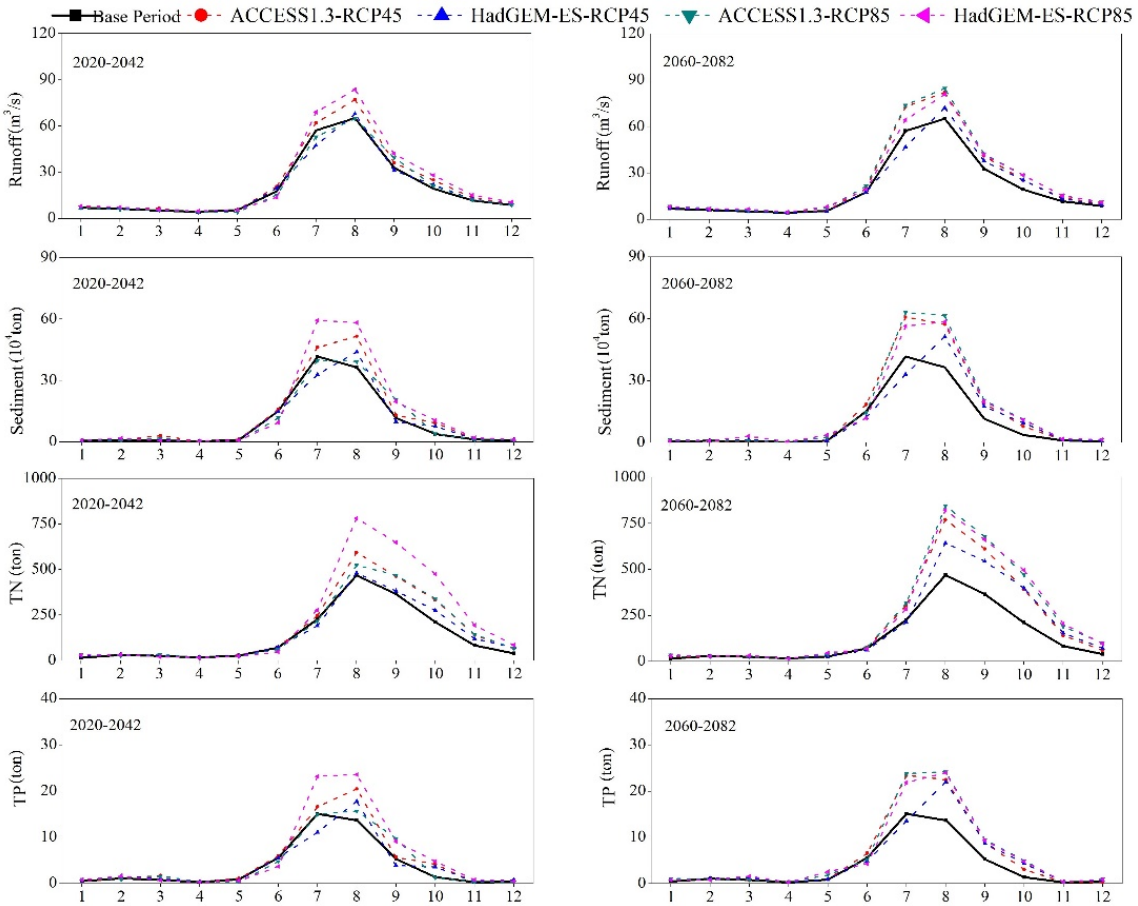

Figure 13. Comparison of average monthly streamflow, sediment, total nitrogen and total phosphorus under different climate change projection.

In the future, the spatial distribution of runoff, sediment, total nitrogen and total phosphorus loading in watershed will vary significantly with the evaluation period, emission scenarios and global climate models. During the period from 2060 to 2082, all sub-watersheds in the watershed basically showing an increasing trend; during the period from 2020 to 2042, under HadGEM-RCP4.5 scenario, half of the sub-watersheds in the watershed had runoff, sediment, total nitrogen and total phosphorus showing a decreasing trend. Sub-watersheds with a large increase in pollutants in the future were located mainly in the lower reaches of the Chaohe River Watershed. The results of the ensemble average of the GCM model showed that the evapotranspiration, runoff, total nitrogen and total phosphorus load in the future evaluation period were all greater than the baseline period and the changes in variables from 2060 to 2082 were greater than those in the period from 2020 to 2042.

3.4. Future Land Use Scenarios

Previous studies have used scenario analysis to assess the coupling impact of the future land use and future climate change on the hydrological process and non-point source output of the watershed. In the CLUE-S model, the establishment of scenario plans was mainly accomplished by defining different land use requirements and then combined with the spatial allocation module based on the grid of different land use types in the model to predict land use changes under different scenarios.

Based on the analysis of the land use structure, spatial distribution and change characteristics of the Miyun Reservoir watershed and regional planning, three scenarios were developed. Land use demand under different scenarios is used to input into the CLUE-S model to analyze the future spatial distribution change characteristics. The regional planning and regional policy documents involved in this research include "Chengde City Master Plan (2016–2030)", "Zhangjiakou City Master Plan (2016–2030)", "Beijing City Master Plan (2016–2030)", "Beijing Major Function Zone Planning", "Miyun New Town Planning (2005–2020)", "Chaobai River Green Ecological Development Zone Comprehensive Planning (2010–2020)", "Beijing Miyun Reservoir Huairou Reservoir He Jingmi Water Diversion Canal Protection and Management Regulations".

Three scenarios are proposed as follows shown in Figure 14:

1. Historical trend scenario: The future demand for land use follows the linear change trend of land use from 2000 to 2008. The overall performance of future land use changes is as follows: forest and urban land will increase and the area of grassland, water bodies, unused land and arable land will decrease. This scenario describes a scenario where there is no future intervention in land use change policies.
2. Ecological protection without consideration of spatial allocation scenario: Many water and soil conservation projects are currently being implemented in the Miyun River Watershed, such as: Taihang Mountain Greening Project, Beijing-Tianjin Sand Source Control Project. In the meantime, since the Miyun Reservoir is the source of drinking water in Beijing, environmental protection of the watershed is particularly important. Therefore, in the future, the annual growth rate of forest land, grassland and urban land will be 1.5, 0.5 and 1.5 times the historical trend scenario, respectively.
3. Ecological protection with consideration of spatial allocation scenario: Based on the results of the historical SWAT simulation from 1988 to 2010 and taking into account the spatial output characteristics of non-point source pollution in the watershed under future climate change and the Miyun Reservoir Watershed Protection Zone Division, specific regional preference variables were added to increase the probability of conversion of cultivated land to forest land in the secondary protection areas of the Miyun Reservoir watershed, watersheds above 25 °C and downstream subcatchments of the Miyun Reservoir watershed. In this study, the regional weighting factor for forest land was set at 0.6 and the weighting factor for other land use types was set to 0. The rate of change of the different land use types was consistent with the ecological protection scenarios that did not consider the spatial allocation.

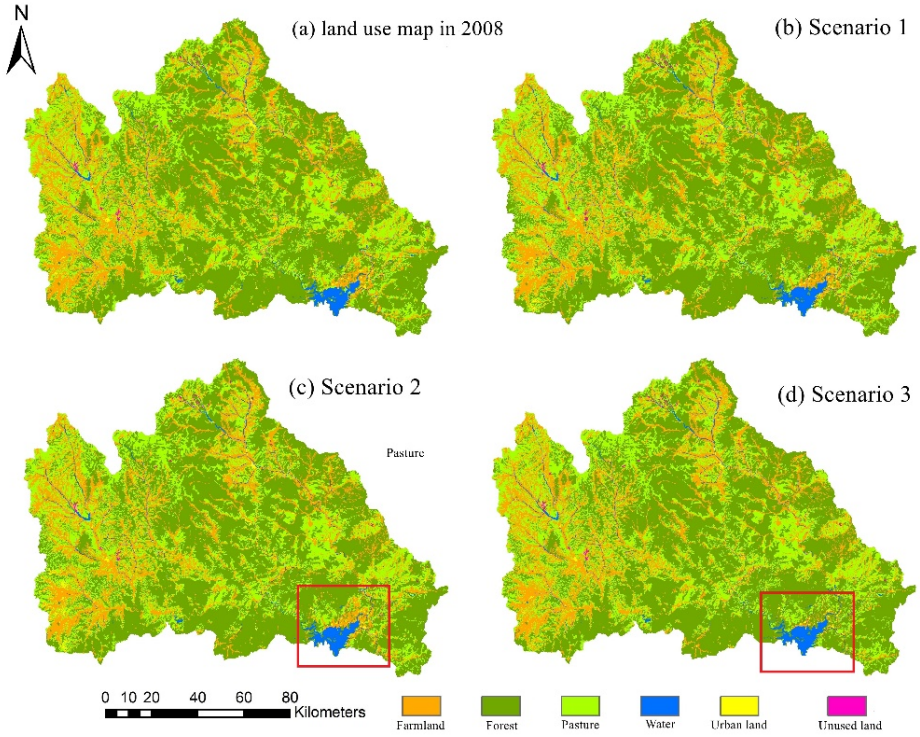

Figure 14. Simulation results for land use under different scenarios in the watershed in 2042. (**a**) land use map in 2008; (**b**) historical trend scenario; (**c**) ecological protection without consideration of spatial configuration scenario; (**d**) ecological protection scenario with more forest.

3.5. Climate Change and Land Use Change Impacts on Streamflow and NPS Loading

After importing the future land use map into the SWAT model database and using the SWAT model to simulate the non-point source pollution load in the Miyun Reservoir watershed, the annual average pollution load in the three land use scenarios was analyzed, noting that the simulation period was from 1988 to 2010. Comparative analysis was used to define the load reduction of sediment, total nitrogen and total phosphorus and the values are shown in Tables 5–7, GCM1 and GCM2 mentioned in the tables stand for ACCESS1.3 and HadGEM-ES, respectively.

The simulation results showed that the ecological protection scenario considering the spatial configuration has a better reduction effect on the output of sediment and nutrients. In the historical reference period, the reductions in sediment, total nitrogen and total phosphorus were 12.88 $\times$ 10^4−ton, 280.918 ton and 8.116 ton, respectively. Under future climate change scenarios, the amount of sediment reduction will increase and the reduction of total nitrogen and total phosphorus will decrease. The average reduction rates of sediment, total nitrogen and total phosphorus were 11.4%, 6.3% and 7.4%, respectively. In the SWAT model, the surface runoff is calculated using the SCS (soil conservation service) method and its runoff will decrease as the value of the runoff curve number decreases. Since the CN value of forest land is smaller than that of cultivated land, the runoff will be reduced after returning farmland to forest. Corresponding reduction, the improvement of soil water retention capacity in the watershed can effectively reduce soil erosion, thereby reducing the output load of sediment; at the same time, as the large area of arable land is reduced, the overall fertilizer use in the watershed will be greatly reduced. The output of nitrogen and phosphorus nutrients will also be greatly reduced. At the same time, in the ecological protection scenario considering the spatial configuration, the sub-watersheds where the pollution load will increase in the future climate change scenario are considered, which will help to further reduce the sediment and nutrients.

Table 5. Reduction of NPS pollution loads by land use change of historical trend scenarios.

Variable	History	2020–2042				2060–2082			
		RCP4.5		RCP8.5		RCP4.5		RCP8.5	
		GCM1	GCM2	GCM1	GCM2	GCM1	GCM2	GCM1	GCM2
Sediment reduction	−4.7	−23.01	−31.26	−30.05	−6.19	−12.76	−16.1	−6.41	−5.89
Sediment reduction rate	−4.10%	−15.9%	−27.0%	−24.8%	−3.8%	−7.5%	−12.3%	−3.5%	−3.5%
Total nitrogen reduction	248.74	−60.53	−208.15	−130.34	173.11	71.49	20.18	214.54	201.87
Total nitrogen reduction rate	15.70%	−3.0%	−12.1%	−6.7%	6.6%	2.9%	0.9%	7.6%	7.2%
Total phosphorus reduction	7.44	−6.23	−10.84	−9.45	0.74	−2.32	−2.39	1.13	1.06
Total phosphorus reduction rate	16.30%	−10.7%	−22.9%	−18.5%	1.1%	−3.4%	−4.1%	1.5%	1.5%

Table 6. Reduction of NPS pollution loads by land use change of ecological protection without the consideration of spatial allocation scenario.

Variable	History	2020–2042				2060–2082			
		RCP4.5		RCP8.5		RCP4.5		RCP8.5	
		GCM1	GCM2	GCM1	GCM2	GCM1	GCM2	GCM1	GCM2
Sediment reduction	−10.15	−9.68	−9.56	−11.59	−10.45	−12.74	−9.76	−10.63	−9.69
Sediment reduction rate	−8.90%	−6.7%	−8.3%	−9.6%	−6.3%	−7.5%	−7.5%	−5.9%	−5.7%
Total nitrogen reduction	218.81	417.82	343.04	429.56	643.86	595.69	518.67	701.03	737.87
Total nitrogen reduction rate	13.80%	20.4%	19.9%	22.0%	24.5%	24.0%	23.4%	24.8%	26.5%
Total phosphorus reduction	6.17	−4.13	−4.46	−4.59	−4.30	−5.16	−3.77	−4.74	−3.49
Total phosphorus reduction rate	13.50%	−7.1%	−9.4%	−9.0%	−6.2%	−7.5%	−6.4%	−6.4%	−4.9%

Table 7. Reduction of NPS pollution loads by land use change of ecological protection with the consideration of spatial allocation scenario.

Variable	History	2020–2042				2060–2082			
		RCP4.5		RCP8.5		RCP4.5		RCP8.5	
		GCM1	GCM2	GCM1	GCM2	GCM1	GCM2	GCM1	GCM2
Sediment reduction	12.88	16.96	15.17	14.75	18.24	18.29	14.23	19.4	18.96
Sediment reduction rate	11.30%	11.7%	13.1%	12.2%	11.1%	10.8%	10.9%	10.7%	11.2%
Total nitrogen reduction	280.92	115.00	111.82	147.20	164.31	152.22	149.20	171.37	187.73
Total nitrogen reduction rate	17.80%	5.6%	6.5%	7.5%	6.2%	6.1%	6.7%	6.1%	6.7%
Total phosphorus reduction	8.12	4.44	3.89	4.00	5.05	4.90	4.21	5.24	5.24
Total phosphorus reduction rate	17.80%	7.6%	8.2%	7.8%	7.2%	7.1%	7.1%	7.1%	7.3%

Note: The unit of sediment reduction is 10^4 ton and the unit of total nitrogen and total phosphorus reduction is ton.

4. Conclusions

Based on the empirical downscaling method, this study used two typical emission scenarios (RCP4.5 and RCP8.5) and two GCMS (ACCESS1.3 and HadGCM-ES) to generate future climate scenario data for the Miyun Reservoir basin. In general, the future climate will show a trend of warming and humidification.

It was found that future changes in the spatial distribution of watershed runoff, sediment, total nitrogen and total phosphorus load in the watershed will differ greatly depending on the evaluation period, emission scenarios and global climate models. During the period from 2060 to 2082, all sub-basins in the basin basically showed an increasing trend; during the period from 2020 to 2042 and under HadGEM-RCP4.5 scenario, half of the sub-basins in the basin had water production, sediment production, total nitrogen and total phosphorus showing a decreasing trend. In addition, the amount of load change showed a decreasing trend. It was also found that sub-basins with a strong increase in pollutants in the future, are mainly located in the lower reaches of the Chaohe River Basin. The results of the GCM ensemble average showed that the evapotranspiration, water production,

total nitrogen and total phosphorus output load in the future evaluation period were all greater than the baseline period and the changes in variables during the period from 2060 to 2082 were greater than the changes in variables from 2020 to 2042.

After assessing the impact of climate change on runoff and NPS loading by the SWAT model, three scenarios were generated by the CLUE-S model to evaluate the reduction of sediment and nutrients in the watershed. After analyzing the relationship between the spatial distribution of land use types and driving factors in historical periods, the integrated impact of climate change and land use was evaluated. The results showed that land use change measures have a good reducing effect on the output of sediment and nutrients. Under ecological protection with consideration of spatial configuration scenario, the average reduction rates of sediment, total nitrogen and total phosphorus, were 11.4%, 6.3% and 7.4%, respectively. These results were explained by the fact that the ecological protection scenario takes fully into account the MRW protection zone policy, the policy of returning farmland to forest and the spatial variation of pollutants in the watershed under future climate scenarios. Therefore, the addition of region-specific preference variables under land use change setting provides better pollutant control effects under future climate scenarios.

Author Contributions: Z.S. proposed the conceptualization and supervised the study; M.F. developed the SWAT model and CLUE-S model, analyzed and discussed the simulation results and drafted the manuscript. Both authors have read and agreed to the published version of the manuscript.

Funding: This research was funded by the Fund for the Innovative Research Group of the National Natural Science Foundation of China (No. 51721093).

Data Availability Statement: The data presented in this study are available upon request from the corresponding author.

Acknowledgments: The authors would like to express their gratitude to EditSprings (https://www.editsprings.com/) for the expert linguistic services provided.

Conflicts of Interest: The authors declare no conflict of interest.

References

1. Ouyang, W.; Hao, F.-H.; Wang, X.; Cheng, H.-G. Nonpoint Source Pollution Responses Simulation for Conversion Cropland to Forest in Mountains by SWAT in China. *Environ. Manag.* **2008**, *41*, 79–89. [CrossRef]
2. Shen, Z.; Liao, Q.; Hong, Q.; Gong, Y. An Overview of Research on Agricultural Non-Point Source Pollution Modelling in China. *Sep. Purif. Technol.* **2012**, *84*, 104–111. [CrossRef]
3. Wu, L.; Long, T.; Liu, X.; Guo, J. Impacts of Climate and Land-Use Changes on the Migration of Non-Point Source Nitrogen and Phosphorus during Rainfall-Runoff in the Jialing River Watershed, China. *J. Hydrol.* **2012**, *475*, 26–41. [CrossRef]
4. Cobb, A.N.; Thompson, J.L. Climate Change Scenario Planning: A Model for the Integration of Science and Management in Environmental Decision-Making. *Environ. Model. Softw.* **2012**, *38*, 296–305. [CrossRef]
5. Wang, Y.; Bian, J.; Zhao, Y.; Tang, J.; Jia, Z. Assessment of Future Climate Change Impacts on Nonpoint Source Pollution in Snowmelt Period for a Cold Area Using SWAT. *Sci. Rep.* **2018**, *8*, 1–13. [CrossRef] [PubMed]
6. Nguyen, H.H.; Recknagel, F.; Meyer, W.; Frizenschaf, J.; Ying, H.; Gibbs, M.S. Comparison of the Alternative Models SOURCE and SWAT for Predicting Catchment Streamflow, Sediment and Nutrient Loads under the Effect of Land Use Changes. *Sci. Total Environ.* **2019**, *662*, 254–265. [CrossRef] [PubMed]
7. Yang, H.; Wang, G.; Wang, L.; Zheng, B. Impact of Land Use Changes on Water Quality in Headwaters of the Three Gorges Reservoir. *Environ. Sci. Pollut. Res.* **2016**, *23*, 11448–11460. [CrossRef]
8. Zhang, L.; Lu, W.; An, Y.; Li, D.; Gong, L. Response of Non-Point Source Pollutant Loads to Climate Change in the Shitoukoumen Reservoir Catchment. *Environ. Monit. Assess.* **2012**, *184*, 581–594. [CrossRef] [PubMed]
9. Narsimlu, B.; Gosain, A.K.; Chahar, B.R. Assessment of Future Climate Change Impacts on Water Resources of Upper Sind River Watershed, India Using SWAT Model. *Water Resour. Manag.* **2013**, *27*, 3647–3662. [CrossRef]
10. Li, T.; Kim, G. Impacts of Climate Change Scenarios on Non-Point Source Pollution in the Saemangeum Watershed, South Korea. *Water* **2019**, *11*, 1982. [CrossRef]
11. Wang, Q.; Liu, R.; Men, C.; Guo, L. Application of Genetic Algorithm to Land Use Optimization for Non-Point Source Pollution Control Based on CLUE-S and SWAT. *J. Hydrol.* **2018**, *560*, 86–96. [CrossRef]
12. Wang, Q.; Liu, R.; Men, C.; Guo, L.; Miao, Y. Effects of Dynamic Land Use Inputs on Improvement of SWAT Model Performance and Uncertainty Analysis of Outputs. *J. Hydrol.* **2018**, *563*, 874–886. [CrossRef]

13. Bai, Y.; Ochuodho, T.O.; Yang, J. Impact of Land Use and Climate Change on Water-Related Ecosystem Services in Kentucky, USA. *Ecol. Indic.* **2019**, *102*, 51–64. [CrossRef]
14. Bai, X.; Shen, W.; Wang, P.; Chen, X.; He, Y. Response of Non-Point Source Pollution Loads to Land Use Change under Different Precipitation Scenarios from a Future Perspective. *Water Resour. Manag.* **2020**, *34*, 3987–4002. [CrossRef]
15. Liu, R.; Zhang, P.; Wang, X.; Chen, Y.; Shen, Z. Assessment of Effects of Best Management Practices on Agricultural Non-Point Source Pollution in Xiangxi River Watershed. *Agric. Water Manag.* **2013**, *117*, 9–18. [CrossRef]
16. Xie, H.; Chen, L.; Shen, Z. Assessment of Agricultural Best Management Practices Using Models: Current Issues and Future Perspectives. *Water* **2015**, *7*, 1088–1108. [CrossRef]
17. Jang, S.S.; Ahn, S.R.; Kim, S.J. Evaluation of Executable Best Management Practices in Haean Highland Agricultural Catchment of South Korea Using SWAT. *Agric. Water Manag.* **2017**, *180*, 224–234. [CrossRef]
18. Kaini, P.; Artita, K.; Nicklow, J.W. Optimizing Structural Best Management Practices Using SWAT and Genetic Algorithm to Improve Water Quality Goals. *Water Resour. Manag.* **2012**, *26*, 1827–1845. [CrossRef]
19. Jeon, D.J.; Ki, S.J.; Cha, Y.; Park, Y.; Kim, J.H. New Methodology of Evaluation of Best Management Practices Performances for an Agricultural Watershed According to the Climate Change Scenarios: A Hybrid Use of Deterministic and Decision Support Models. *Ecol. Eng.* **2018**, *119*, 73–83. [CrossRef]
20. Yan, T.; Bai, J.; Lee Zhi Yi, A.; Shen, Z. SWAT-Simulated Streamflow Responses to Climate Variability and Human Activities in the Miyun Reservoir Watershed by Considering Streamflow Components. *Sustainability* **2018**, *10*, 941. [CrossRef]
21. Xu, Z.X.; Pang, J.P.; Liu, C.M.; Li, J.Y. Assessment of Runoff and Sediment Yield in the Miyun Reservoir Catchment by Using SWAT Model. *Hydrol. Process.* **2009**, *23*, 3619–3630. [CrossRef]
22. Bai, J.; Shen, Z.; Yan, T. A Comparison of Single- and Multi-Site Calibration and Validation: A Case Study of SWAT in the Miyun Reservoir Watershed, China. *Front. Earth Sci.* **2017**, *11*, 592–600. [CrossRef]
23. Eum, H.-I.; Gupta, A.; Dibike, Y. Effects of Univariate and Multivariate Statistical Downscaling Methods on Climatic and Hydrologic Indicators for Alberta, Canada. *J. Hydrol.* **2020**, *588*, 125065. [CrossRef]
24. Chen, H.; Xu, C.-Y.; Guo, S. Comparison and Evaluation of Multiple GCMs, Statistical Downscaling and Hydrological Models in the Study of Climate Change Impacts on Runoff. *J. Hydrol.* **2012**, *434–435*, 36–45. [CrossRef]
25. Wang, L.; Ranasinghe, R.; Maskey, S.; Van Gelder, P.H.A.J.M.; Vrijling, J.K. Comparison of Empirical Statistical Methods for Downscaling Daily Climate Projections from CMIP5 GCMs: A Case Study of the Huai River Watershed, China. *Int. J. Climatol.* **2016**, *36*, 145–164. [CrossRef]
26. Xu, C. From GCMs to River Flow: A Review of Downscaling Methods and Hydrologic Modelling Approaches. *Prog. Phys. Geogr. Earth Environ.* **1999**, *23*, 229–249. [CrossRef]
27. Abatzoglou, J.T.; Brown, T.J. A Comparison of Statistical Downscaling Methods Suited for Wildfire Applications. *Int. J. Climatol.* **2012**, *32*, 772–780. [CrossRef]
28. Cannon, A.J.; Sobie, S.R.; Murdock, T.Q. Bias Correction of GCM Precipitation by Quantile Mapping: How Well Do Methods Preserve Changes in Quantiles and Extremes? *J. Clim.* **2015**, *28*, 6938–6959. [CrossRef]
29. Ngai, S.T.; Tangang, F.; Juneng, L. Bias Correction of Global and Regional Simulated Daily Precipitation and Surface Mean Temperature over Southeast Asia Using Quantile Mapping Method. *Glob. Planet. Chang.* **2017**, *149*, 79–90. [CrossRef]
30. Yan, T.; Bai, J.; Arsenio, T.; Liu, J.; Shen, Z. Future Climate Change Impacts on Streamflow and Nitrogen Exports Based on CMIP5 Projection in the Miyun Reservoir Basin, China. *Ecohydrol. Hydrobiol.* **2019**, *19*, 266–278. [CrossRef]
31. Zheng, F.; Hu, Y. Assessing Temporal-Spatial Land Use Simulation Effects with CLUE-S and Markov-CA Models in Beijing. *Environ. Sci. Pollut. Res.* **2018**, *25*, 32231–32245. [CrossRef] [PubMed]
32. Qiu, J.; Shen, Z.; Chen, L.; Hou, X. Quantifying Effects of Conservation Practices on Non-Point Source Pollution in the Miyun Reservoir Watershed, China. *Environ. Monit. Assess.* **2019**, *191*, 1–21. [CrossRef] [PubMed]
33. Jia, K.; Ruan, Y.; Yang, Y.; Zhang, C. Assessing the Performance of CMIP5 Global Climate Models for Simulating Future Precipitation Change in the Tibetan Plateau. *Water* **2019**, *11*, 1771. [CrossRef]
34. Bao, Z.; Fu, G.; Wang, G.; Jin, J.; He, R.; Yan, X.; Liu, C. Hydrological Projection for the Miyun Reservoir Watershed with the Impact of Climate Change and Human Activity. *Quat. Int.* **2012**, *282*, 96–103. [CrossRef]
35. Sun, Q.; Miao, C.; Duan, Q. Comparative Analysis of CMIP3 and CMIP5 Global Climate Models for Simulating the Daily Mean, Maximum and Minimum Temperatures and Daily Precipitation over China. *J. Geophys. Res. Atmos.* **2015**, *120*, 4806–4824. [CrossRef]